THE PENNSYLVANIA
STATE UNIVERSITY

IONOSPHERIC RESEARCH

Scientific Report No. 345

AN INVESTIGATION OF TRANSIENT MAGNETIC FIELDS IN A PLASMA TRAPPED IN A DIPOLAR MAGNETIC FIELD

by
R. H. Garvey

December 10, 1969

IONOSPHERE RESEARCH LABORATORY

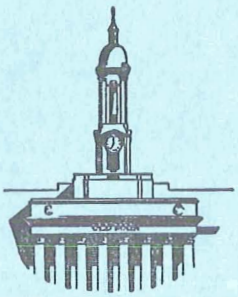

University Park, Pennsylvania NASA Grant NGL-39-009-003

Ionospheric Research

NASA Grant NGL-39-009-003

Scientific Report

on

"An Investigation of Transient Magnetic Fields in a Plasma Trapped in a Dipolar Magnetic Field"

by

R. H. Garvey

December 10, 1969

Scientific Report No. 345

Submitted by:

John S. Nisbet, Professor of Electrical Engineering
Project Supervisor

The Pennsylvania State University

TABLE OF CONTENTS

ABSTRACT

Instability discharges accompanying steady-state plasmas trapped in a steady-state magnetic field are described and studied. It is possible that these transient discharges may be similar to certain aspects of auroral phenomena. Spatial mappings of the transient magnetic fields associated with these instabilities are presented, along with qualitative discussions concerning the origins of the instabilities.

1. Introduction

1.1 The Basic Phenomena

With a spherical dipolar magnet serving as the cathode, a steady-state glow discharge having several unique features can be established. The plasma formed in such a discharge is trapped in the magnetic field of the sphere and, as a result of this trapping, the plasma can assume the form of a flat belt in the equatorial plane of the sphere. Within a certain range of pressures and discharge voltages and for a sufficiently large sphere, this steady-state plasma belt is accompanied by arc instabilities which appear to originate in the plasma belt and propagate along the magnetic field lines to the surface of the sphere. These arcs are produced by highly energetic ions and electrons and, therefore, may be considered to be localized, transient currents. Each such current or arc has an associated transient magnetic field. The spatial and temporal variation of these fields has been determined using a small coil placed in the vicinity of the arcs. These measurements, together with a description of the principal characteristics of both the steady-state glow discharge and the arc instabilities, will be presented.

1.2 Previous Related Work

The experimental configuration and technique described above for obtaining a steady-state plasma trapped in a dipolar magnetic field was first presented by (Quinn and Chang, 1966). (Quinn, 1966)

reported on the arc instabilities that may accompany the trapped plasma. An article written by (Quinn and Fiorito, 1967) contains descriptions of some of the properties of both the steady-state plasma belt and the arcs. This article also contains plots of the transient time behavior of the electric potential with respect to ground of various points in the plasma belt as a result of the arc instabilities. (Twardeck, 1968) used this same discharge configuration to investigate the scattering of microwaves by a steady-state plasma trapped in a dipolar magnetic field. Noise measurements of this discharge by (Schmidt, 1969) indicate that the steady-state plasma oscillates at frequencies in the kilohertz range.

The use of a small coil to measure time-varying magnetic fields in a plasma is a standard diagnostic technique. Two of the main uses of such magnetic probes are to measure the magnetic fields associated with the plasma current in a pulsed discharge and to measure the magnetic field associated with a pinched discharge. The work of (Lovberg, 1964) is an example of the former and that of (Tuck, 1959) an example of the latter application.

There is little reported in the literature concerning the measurement of magnetic fields associated with currents which are both spatially and temporally random. The fact that the arc instabilities observed in this work have a random character in space and in time necessitated special experimental methods which will be described later in this work.

1.3 Definitions of Symbols

In this section, the definitions of the symbols used in this work are presented. The symbols are arranged alphabetically in order of Latin letters and then Greek letters.

$\vec{B}$ ≡ magnetic flux density vector

B_i ≡ i^{th} component of $\vec{B}$

$B_{i_{MAX}}$ ≡ maximum value with respect to time of B_i obtained at a given location in the plasma for a given set of discharge conditions

$\frac{d\vec{B}}{dt}$ ≡ derivative with respect to time of $\vec{B}$

$\frac{dB_i}{dt}$ ≡ i^{th} component of $\frac{d\vec{B}}{dt}$

$\frac{dB_i}{dt_{MAX}}$ ≡ maximum value with respect to time of $\frac{dB_i}{dt}$ obtained at a given location in the plasma for a given set of discharge conditions

I_D ≡ discharge current: the current flowing between the anode and cathode of the discharge

P ≡ pressure inside the bell jar of the vacuum system

r ≡ radial distance between the surface of the sphere and the geometric center of the coil

V_D ≡ discharge voltage: the voltage between the cathode and anode of the discharge

θ ≡ colatitudinal angle in spherical coordinates

ϕ ≡ azimuthal angle in spherical coordinates

ρ ≡ radial variable in spherical coordinates

2. Experimental Aspects

2.1 Experimental Apparatus

The basic phenomenon in the experiment consists of a steady-state plasma trapped in a dipolar magnetic field. The source of the magnetic field is a uniformly magnetized metallic sphere. The sphere used in this experiment is made of Alnico V and is 15.2 centimeters in diameter. The sphere's magnetic field varies from 435 gauss at one-half a centimeter from the sphere's surface to 20 gauss at 15 centimeters in the equatorial plane of the sphere. Figure 2.1 shows a plot of this variation of the sphere's magnetic field with distance from the sphere. The magnetic field of the sphere was measured with a Bell gaussmeter, Model 620.

The magnetized sphere is placed inside a vacuum chamber consisting of a base plate, 51 centimeters in diameter, and a removable Pyrex-glass bell jar, 81 centimeters high and 46 centimeters in diameter. The sphere is attached to a rod so that the sphere's magnetic poles are vertically above one another. Thus, the equatorial plane of the sphere is a horizontal plane through the center of the sphere. The rod to which the sphere is attached insulates the sphere from the base plate. This vacuum chamber is part of a Veeco VS-400 vacuum system which is capable of reaching pressures as low as 5 microns with its mechanical roughing pump. This minimum pressure is low enough for the purposes of the experiment described in this work. All pressures are measured with conventional thermocouple

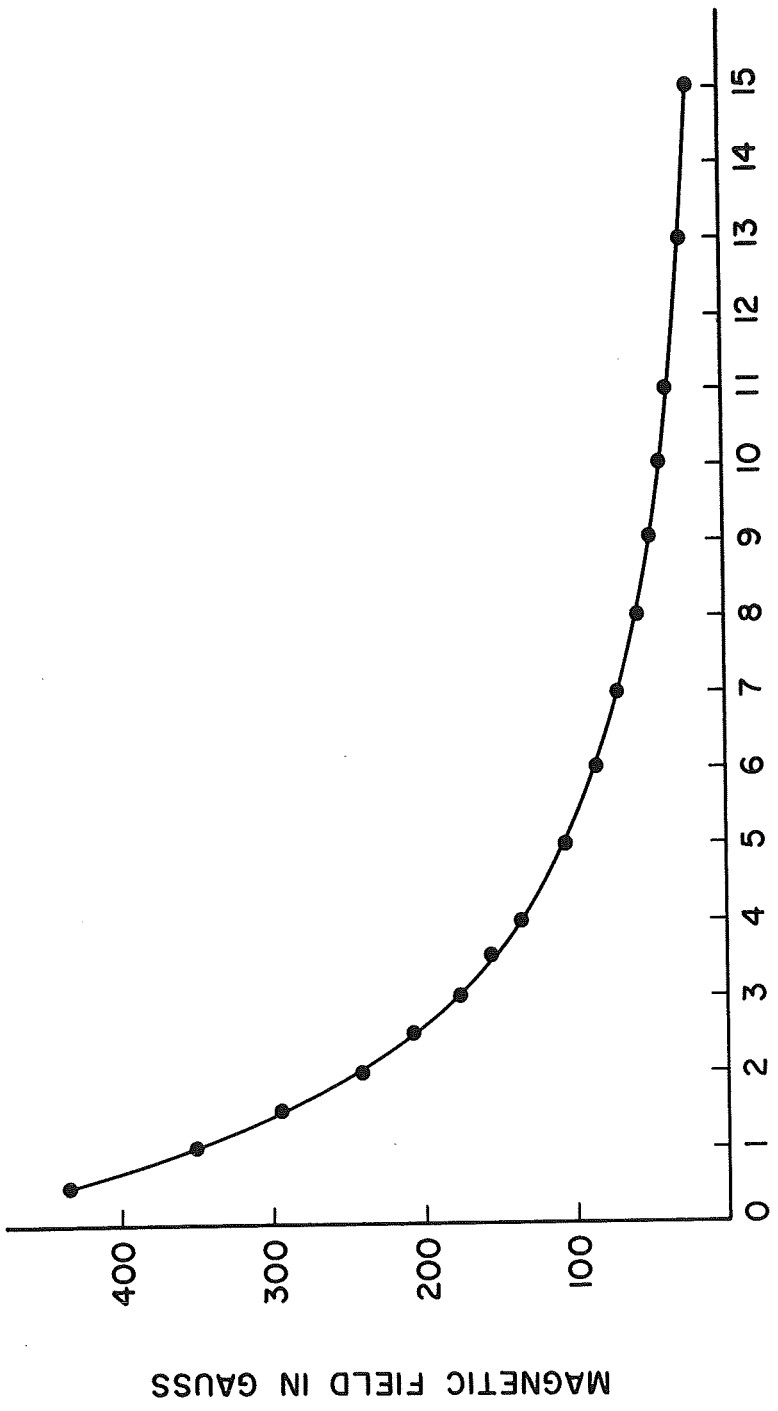

Figure 2.1 Radial Variation of the Sphere's Magnetic Field

gauges which are part of the vacuum system. Figure 2.2 is a photograph of the vacuum system with the sphere in position inside the bell jar.

The sphere serves as the cathode in forming the glow discharge used in this experiment. A loop of wire around the inside of the vacuum system's bell jar is used as the anode in the discharge. By using a D.C. power supply, a continuous glow discharge can be maintained between the sphere and the wire ring. A current-limiting, 165K resistor is placed in series with the discharge to protect the power supply, which could produce a maximum current of 10 milliamperes, and to ensure that the discharge would occur at fairly low supply voltages, about four to five hundred volts.

A small coil 0.75 centimeters in diameter is used to measure the transient magnetic fields that arise as a result of arc instabilities in the glow discharge. This coil is placed atop a plexiglass stand which slides on a track placed on the base plate of the vacuum chamber. The track is positioned so that the stand and coil can slide in and out from the sphere in a direction along a radius from the center of the sphere. In this way, a complete mapping of a component of $\frac{d\vec{B}}{dt}$ in a horizontal plane about the sphere can be obtained for a given coil orientation without necessitating the removal of the bell jar to adjust the coil's orientation each time after the coil's position is changed. Figure 2.3 shows a photograph of this sliding-stand arrangement with the coil in place. The sliding stand is activated by a rotary feed-through in the base plate.

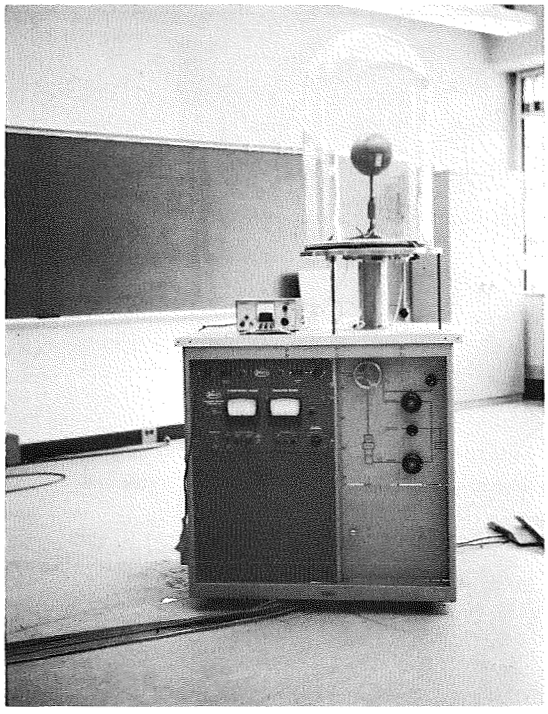

Figure 2.2 The Basic Experimental Apparatus

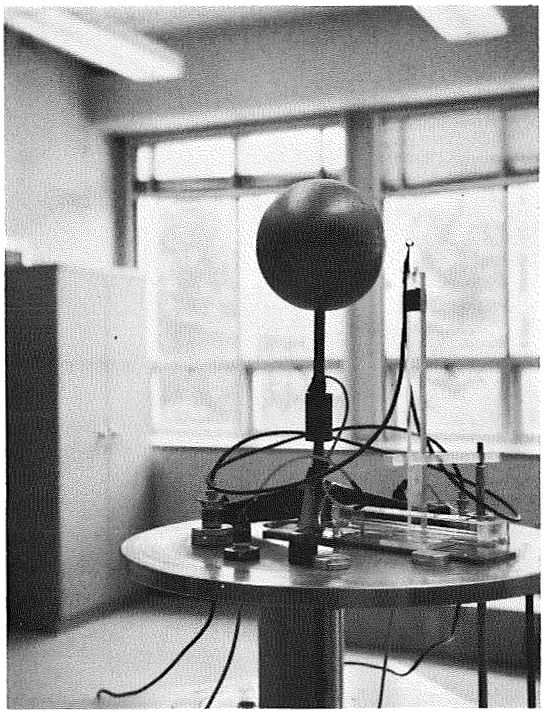

Figure 2.3 Sliding Stand and Sphere

The signals from the coil are fed into a Type D Tektronix plug-in unit which is inserted into a Type 544 Tektronix oscilloscope. The displayed coil signal is recorded photographically.

2.2 Observed Plasma Phenomena

In this section, the general characteristics of the steady-state plasma are described. Next, the three types of arc instabilities which may accompany the steady-state discharge are described together with the discharge conditions for which each of these types of arc is the dominant one occurring. Last, the effects of discharge current, pressure, and the sphere's surface condition on the generation of the flash-like arcs are investigated.

2.2.1 Steady-State Glow Discharge

With the magnetized sphere serving as the cathode and a ring of wire around the inside of the bell jar as the anode, a steady-state discharge can be established and maintained between the sphere and the wire. The shape of this discharge varies somewhat with pressure and discharge voltage. At pressures above 200 microns and supply voltages of about 450 volts, the plasma covers the upper part of the sphere and extends visibly only a few centimeters out from the surface of the sphere. At supply voltages above 500 volts and at pressures below 200 microns, however, the discharge assumes the shape of a flat belt confined to the equatorial plane of the sphere as a result of the trapping effect of the sphere's magnetic field on the plasma. The belt flattens even more as the pressure is lowered further. This plasma belt extends visibly from about one centimeter from the sphere's

surface out to the wire-ring anode. The belt has the fundamental characteristics of a glow discharge with a cold cathode. A picture of the steady-state plasma belt is presented in Figure 4.

This plasma belt will be formed regardless of the physical geometry of the anode used. The belt will be principally confined to the sphere's equatorial plane whether the anode is a wire ring or just a wire tip placed in the vicinity of the sphere. It is the sphere's magnetic field that determines the shape of the trapped plasma. A ring of wire is used as the anode in this experiment because this configuration seems to produce a fairly stable plasma belt.

In all the experiments described herein, the discharge is always formed in an air atmosphere. It has been found that the neutral background constituent has little effect on the nature and formation of the belt.

Previous measurements (Quinn and Fiorito, 1967) indicate that the temperature in this plasma belt varies with radial distance from the sphere's surface from a maximum of 10 electron volts at about 2 centimeters from the sphere to 1 electron volt at 13 centimeters. The charged-particle density varies from a maximum of 10^7 particles per $(\text{centimeter})^3$ at 5 centimeters from the sphere to 10^5 particles per $(\text{centimeter})^3$ at 13 centimeters.

2.2.2 Arc Instabilities in the Glow Discharge

At supply voltages above 600 volts and pressures below 400 microns, the steady-state plasma ring is accompanied by arc

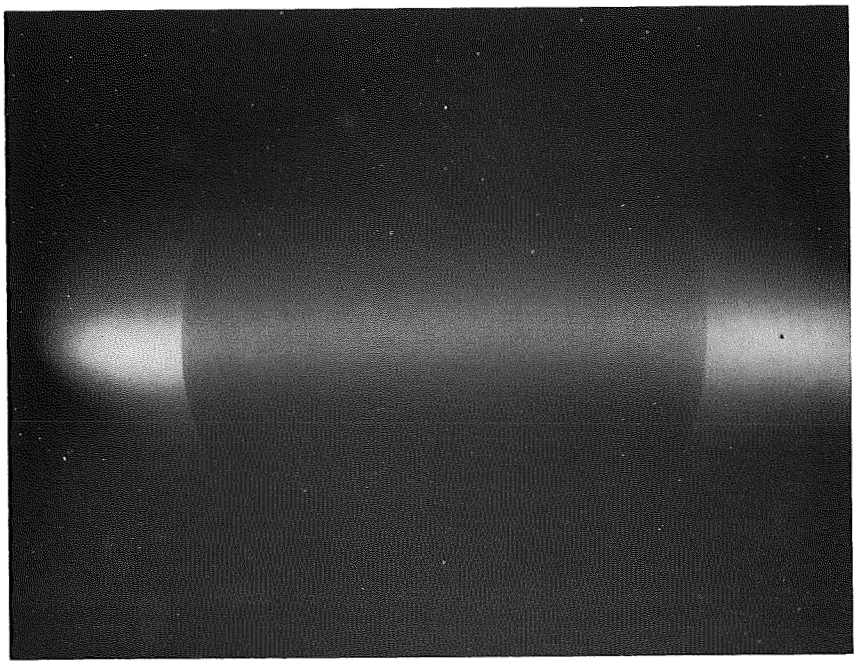

Figure 2.4 Steady-State Plasma Belt

instabilities which, from visual observation, appear to originate in the plasma belt and propagate along the sphere's magnetic field line to the surface of the sphere. These arcs may extend from the plasma toward the lower, upper, or both hemispheres of the sphere.

There are three kinds of arc instabilities that may arise in the plasma belt. Figures 2.5, 2.6, and 2.7 are photographs of each of these types of arcs. The three types may be classified according to their physical length, their brightness, and their time of duration. Under proper conditions of pressure and discharge current, all three kinds of arcs may occur together in the plasma, but one can usually vary the pressure-current conditions so that any one of the three will appear by itself.

One type of arc consists of long streamers that extend along the sphere's magnetic field lines from the plasma in the equatorial plane to the polar regions of the sphere. Figure 2.5 shows a picture of these streamers. The streamers remain spatially fixed for several seconds at a time. They usually occur at pressures between 50 and 200 microns and at supply voltages below 600 volts. The streamers are the faintest of the arcs.

A second type of arc appearing in the plasma is the small, spark-like arc which occurs within 2 centimeters of the sphere's surface. Figure 2.6 pictures these short arcs which are only a few centimeters in length. As the photograph indicates, these spark-like arcs occur exclusively in the equatorial region of the sphere. These arcs last for only a few microseconds. They usually occur at supply

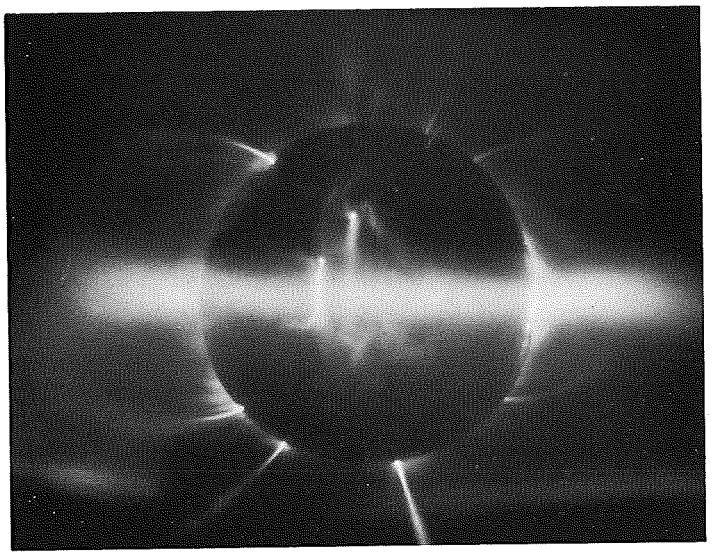

Figure 2.5 Streamers

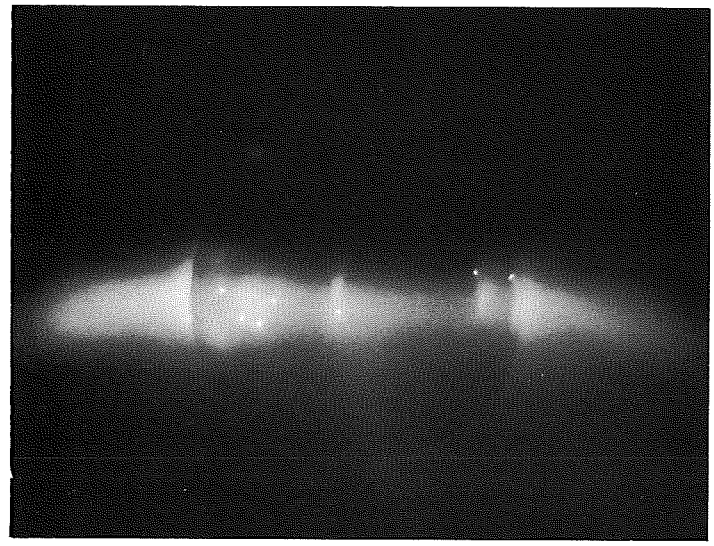

Figure 2.6 Spark-Like Arcs

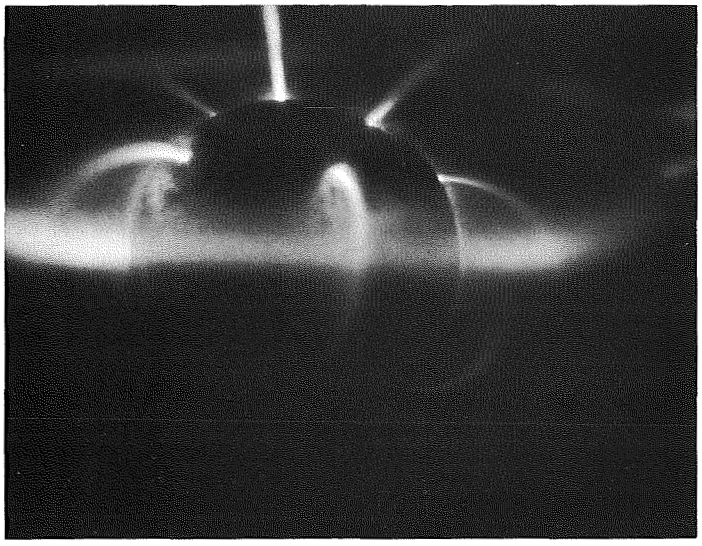

Figure 2.7 Flash-Like Arcs

voltages above 700 volts and at pressures above 50 microns. At pressure above 200 microns or at supply voltages above 900 volts, these arcs are usually the only ones occurring.

The third kind of arc consists of brilliant flashes which travel rapidly from the equatorial plasma belt to the sphere's surface along the magnetic field lines. Figure 2.7 is a photograph of these flash-like arcs. The flash-like arcs have lifetimes of several microseconds and vary in length from a few centimeters to over 10 centimeters depending on their point of origin in the plasma belt. These arcs may strike the sphere anywhere but the majority of them hit the sphere in the regions between 30° and 70° north and south latitudes. The flash-like arcs may be distinguished from the other two types in that they are much brighter and last for a shorter time than the streamers and they are much longer than the spark-like arcs.

The flash-like arcs usually occur at pressures below 200 microns and at supply voltages between 600 and 900 volts. Below 100 microns for supply voltages below 900 volts, they are the principal type of arc instability occurring. It is these flash-like arcs with which the present work deals so the properties of these arcs will be presented in some detail. Any reference below to arcs refers to these flash-like arcs, unless otherwise stated.

The frequency of occurrence of the arcs at a given pressure increases with increasing discharge current. At currents above 0.50 milliamperes and pressures below 50 microns, there are well over a hundred arcs per second occurring in the plasma.

There is only a small range of pressures in which the flash-like arcs occur in abundance and with any sort of consistent characteristics. In fact, at pressures above 25 microns, the arcs often cease to occur after the plasma is sustained for several hours. At pressures below 10 microns, the frequency of the arcs' occurrences begins to fall off noticeably. Thus, the optimum range of pressures for production of the arcs is between 10 and 25 microns.

Under all pressure-current conditions, the arcs occur in a random manner with respect to both time of occurrence and point of origin in the plasma belt. Efforts to produce a flash-like arc at a certain point in the plasma at a certain time have been unsuccessful although the streamers have been produced at a particular position. As was mentioned above, the arcs seem to be generated in the equatorial plasma belt. Evidence for this lies in the fact that at low pressures, about 20 microns, and relatively low supply voltages, about 500 volts, the plasma belt will sometimes flicker as an arc arises in the plasma. In fact, the entire discharge will occasionally be quenched upon the formation of an arc.

2.2.3 Surface Effects

There is experimental evidence indicating that the production of arcs is dependent on the condition of the surface of the magnetized sphere. When the surface of the sphere is polished with emory cloth and cleaned with acetone, it is found that initially only the spark-like arcs appear under pressure-current conditions which normally lead

to the abundant production of the flash-like arcs. The flash-like arcs do not appear until the sphere's surface is scratched in many places with a file, and a film which the discharge always seems to deposit on the sphere is allowed to collect on the sphere's surface. The discharge must be sustained for several hours total time before enough of this dull brown film collects on the sphere to noticeably enhance the arc production.

The unfortunate thing is that as this film continues to collect on the sphere, the arc production is eventually adversely affected by the film's presence. After about two months with the discharge sustained for several hours a day, the flash-like arcs cease to occur at pressures and discharge currents at which the arcs had previously appeared profusely. Thus, in small portions, the film is necessary for the production of the flash-like arcs, but, in too large quantities, the film acts like a dielectric coating on the sphere and inhibits and eventually totally stops the production of the arcs. This was verified by the fact that when the sphere was covered with a dielectric material with a small strip of metal left exposed so the discharge could be sustained, no flash-like arcs occurred. As will be discussed later, the arcs are thought to be caused by an instability arising in the equatorial current which causes a potential to be built up between a point in the equatorial plane and another on the sphere's surface along a field line. This mechanism is consistent with the observed effects of surface conductivity on arc production. At high

conductivity, corresponding to the cleaned surface, not enough potential difference can be built up along the field line to ignite an arc due to continuous leakage current along the field line. At low conductivity, corresponding to the dielectric-coated sphere, the breakdown potential of the arc path is higher than that which can be generated by the instability mechanism. In the intermediate case, conditions are proper for arc ignition. Fortunately, the build-up of film on the sphere's aurface is slow enough so that one has time of the order of days to obtain reproducible experimental conditions to study the properties of the arcs.

2.3 Theory and Coil Design

To measure the transient magnetic field, a small coil is inserted into the plasma. From Faraday's Law, one knows that the voltage induced in such a coil by a time-varying magnetic field $\frac{d\vec{B}}{dt}$ is related to $\frac{d\vec{B}}{dt}$ by:

$$V_c = n A \frac{dB_i}{dt} \quad ,$$

where the subscript i refers to the component of $\frac{d\vec{B}}{dt}$ normal to the coil's circular cross section, n is the number of turns in the coil, and A is the area of the cross section. If A is in $(\text{meters})^2$ and V_c, the voltage induced in the coil, is in volts, then $\frac{dB_i}{dt}$ has units of 10^4 gauss per second. This coil technique measures only time-varying magnetic fields as the constant background magnetic field of the sphere has no effect on the coil's magnetic field measurements.

There are several factors to consider in the design of the coil to be used to measure such transient magnetic fields. First, the characteristic time associated with the frequency response of a coil is $\tau = \frac{L}{R_o}$, where R_o is the external resistance at the output of the coil and L is the inductance of the coil. This inductance is equal to Kn^2r, where K is a constant dependent on the cross-sectional area of the wire of the coil, and r is the radius of the coil's circular cross section. Since one would like τ to be as small as possible for good frequency response, it is desirable to use thin wire of gauge greater than #30 and for n and r to be as small as possible so τ will be small. On the other hand, V_c is proportional to nr^2 and one needs a signal large enough to be detectable. Thus, one would like both n and r to be large. Obviously, one must compromise between the demands of good coil frequency response and large signal output of the coil. In addition, the larger the coil is, the more it will disturb the plasma into which it is inserted. The coil used in this experiment is designed with the criteria that it have the smallest possible physical dimensions and still produce a detectable signal of at least a few millivolts in regions of the plasma belt where the signal from the coil is a minimum.[1]

---

[1] Plasma Diagnostic Techniques, ed. by R. Huddlestone and S. Leonard, pp. 72-73. These pages treat the same coil-design considerations as those presented above.

2.4 Effects of Electric Fields

Besides the considerations of the physical dimensions of the coil, there is also the problem of eliminating electric field effects from the coil's output signal. These spurious electric field effects are the result of a capacitive breakdown between the insulation around the coil wire and the wire itself. This breakdown can occur because of the large potential difference that may exist between the plasma around the coil's insulation and the wire. Since the discharge voltages used in this experiment are about 500 volts, it is essential to eliminate these spurious effects.

There are several standard techniques used to eliminate electric field effects. One such technique consists of putting a porcelain jacket or a thick epoxy coating around the coil. Unfortunately, such a jacket or coating greatly increases the dimensions that the coil presents to the plasma and, therefore, also increases the coil's perturbing effect on the plasma. Since it is felt that the smallest possible coil will give the most accurate mapping of the arc's magnetic fields and will least inhibit or perturb the production of the arcs, the jacket technique is not used in this experiment.

Another method for eliminating electric field effects is that of surrounding the coil with a grounded cage of wires or with a slotted shield. Such a device keeps all electric field effects from the coil but permits the magnetic field to penetrate to the coil through the slots in the metal. Like an insulating jacket, a shield

or cage of wires around the coil prevents an accurate mapping of the arc's magnetic field since the shield prevents arcs from occurring right next to the coil because of the shield's physical size and by its perturbing effect on the plasma. Thus, the shield technique was not used in this experiment.

A third technique, the one used in this experiment, involves the use of a double coil with a grounded center tap. The double coil consists of two coils, each wound with the same number of turns in the same direction and placed side by side to form one coil. The center of this composite coil, which consists of one end of each of the two smaller, adjacent coils, is grounded. The output of the two coils is fed into a differential amplifier. The two small coils together are still very small in size (0.75 centimeters in diamter), so the electric field effects are the same in each coil and will cancel in the differential amplifier. The time-changing magnetic field, however, induces $+ V_c$ with respect to ground in one coil and $- V_c$ with respect to ground in the other coil as a result of the composite coil's center being grounded. In the differential amplifier, the two signals from the two coils are subtracted one from the other to give a net signal of $V_c - (- V_c) = 2V_c$. Thus, the double coil configuration eliminates all electric field effects and perturbs the plasma the least of any of the techniques described above. This method also allows the possibility of an arc's occurring in close proximity to and even through the coil, thereby permitting a much more accurate mapping of

the transient magnetic fields than do the other techniques described in this section.[2]

The double coil in this experiment is made of two circular coils of ten turns each. Thus, the output of the differential amplifier is that of a single, twenty-turn coil. The two ends of each of the two coils are soldered to RG-58A/U coaxial cables to eliminate any stray capacitance or other electric field effects from these coil wires. A type D Tektronix plug-in unit serves as the differential amplifier in this experiment.

2.5 Measurement Techniques

An accurate spatial mapping of the arc's magnetic field requires that only arcs occurring in close proximity to the coil be observed. Now, the closer an arc is to the coil, the stronger the signal will be; so by setting the triggering level on the oscilloscope at a high level, only those signals from arcs occurring very near the coil will be displayed. The pressure-current conditions in the discharge are selected so that many arcs are occurring per second to ensure that the arcs, with their random nature, will occur near the coil at least several times a minute.

The oscilloscope displays of the coil's signals are recorded photographically by taking five-minute time exposures of all the coil

---

[2] Plasma Diagnostic Techniques, pp. 73-75.

signals appearing. Such a time exposure is taken at each position of the coil for each orientation of the coil in that position. The time exposure photograph provides a picture of the superposition of the many signals, usually well over ten, that are recorded in a five-minute period for a given coil position and orientation. This superposition together with the use of a high triggering level also provides an accurate measurement of the maximum signal for a given coil location and orientation.

It is found that the most reproducible results can be obtained by pumping the system down to a pressure of less than 5 microns for about half an hour before the discharge is turned on. This initial pump-down eliminates any impurities present in the atmosphere inside the bell jar as a result of outgassing of the various pieces of apparatus and tape in the vacuum chamber. After this pump-down, air is slowly bled back into the system through a dessicator until the desired pressure is obtained.

It should be recalled that the voltage across the coil, V_c, is proportional to $\frac{dB_i}{dt}$. In fact, $\frac{dB_i}{dt} = \frac{V_c}{nA}$ in 10^4 gauss per second. Obviously, to obtain $B_i(t)$, one must integrate this signal. Unfortunately, there are certain properties inherent to the $\frac{dB_i}{dt}$ signal which make electronic integration of that signal very impractical. The amplitude of the coil signal is very small with the maximum signal no more than 20 millivolts. The signal itself lasts for only about 5 microseconds. This short time duration implies

that the signal is a high frequency one composed of frequencies of the order of megahertz. Now, the output of an R-C integrator is $V = \frac{1}{RC} \int v(\omega t)dt$ where $RC >> \tau$, the lifetime of the signal. Here, τ is about 10^{-5} seconds, so RC should be about 10^{-3} seconds for accurate integration. However, $\int v(\omega t)dt$ is proportional to $\frac{1}{\omega}$, which is approximately 10^{-6} seconds in this experiment. Thus, an accurate integration of the $\frac{dB_i}{dt}$ signal by an R-C circuit will attenuate the signal by $\frac{1}{RC\omega} \simeq 10^{-3}$. This attenuation reduces the coil signal from millivolts to microvolts, which is too small a signal for the oscilloscope to measure.

Integration by an operational amplifier can eliminate this attenuation problem, but the problem of resetting the amplifier after each arc's signal is integrated arises in place of the former difficulty. Signals due to all arcs, even those occurring far from the coil, are integrated by the operational amplifier. As a result, every arc whose magnetic field induces any voltage at all in the coil will contribute to the output of the operational amplifier. Unless the amplifier can be reset to zero after each and every arc occurs, the signals from the arcs will add together in the integrator and the amplifier will produce progressively larger signals. The random nature of the arcs and the fact that there must be many arcs occurring make this resetting of the operational amplifier after each signal very impractical.

Since both of these techniques of electronic integration proved impractical, the signal proportional to $\frac{dB_i}{dt}$ was recorded and $B_i(t)$ obtained by graphic integration.

2.6 Experimental Errors

There are several experimental uncertainties that must be considered in evaluating the data obtained using the above techniques. The actual distance of the coil's center from the sphere's surface can be determined to within $\pm$ 0.10 centimeters. The orientation of the coil with respect to the sphere's surface may be slightly off so that the direction perpendicular to the coil's circular cross section may not be exactly parallel to the component of $\frac{d\vec{B}}{dt}$ that is being measured. It is estimated that the angle between the normal to the coil's cross section and the i^{th} direction is 0° to within $\pm$ 3.0°. In addition, the center of the coil may not be exactly in the equatorial plane during the measurements. It is estimated that the coil's center is within $\pm$ 0.20 centimeters of the vertical height of the equatorial plane while the measurements are being taken. Because the coil is on a rigid stand that slides in and out along a track, these last two uncertainties concerning the orientation of the coil are systematic errors and they should have no effect on the relative values of the plots of a particular component of the maximum value of $\frac{d\vec{B}}{dt}$ or $\vec{B}$ versus r, the radial distance of the coil from the sphere's surface.

For r less than 3 centimeters, there is an additional uncertainty in the plots of $\left(\frac{dB_i}{dt}\right)_{MAX}$ and $B_{i_{MAX}}$ versus r which are presented in the next chapter. This uncertainty is due to the fact that in the region close to the sphere, the spark-like arcs are occurring along with the flash-like arcs. The signal due to the spark-like arcs is thus superimposed on the flash-like arcs' signal. Figure 2.8 shows the two different signals that are produced by these two different kinds of arcs. This particular photograph shows $\frac{dB_\theta}{dt}$ versus t where $\frac{dB_\theta}{dt}$ is the component of $\frac{d\vec{B}}{dt}$ parallel to the direction of the arcs in the equatorial plane. The vertical scale on the photograph is 2 millivolts per major division and the horizontal scale is 1 microsecond per major division. The discharge conditions under which this photograph was obtained were 20 microns pressure, 1 milliampere discharge current, and r equal to 1 centimeter. The inner family of traces, which crosses zero first, is the signal due to the flash-like arcs, and the outer traces are the signals due to the spark-like arcs. The mixing of these two signals can lead to signals larger than the signal due to the flash-like arcs alone and may account for apparent increases in the values of the maximum values of $\frac{dB_i}{dt}$ and B_i as r is decreased below 3 centimeters.

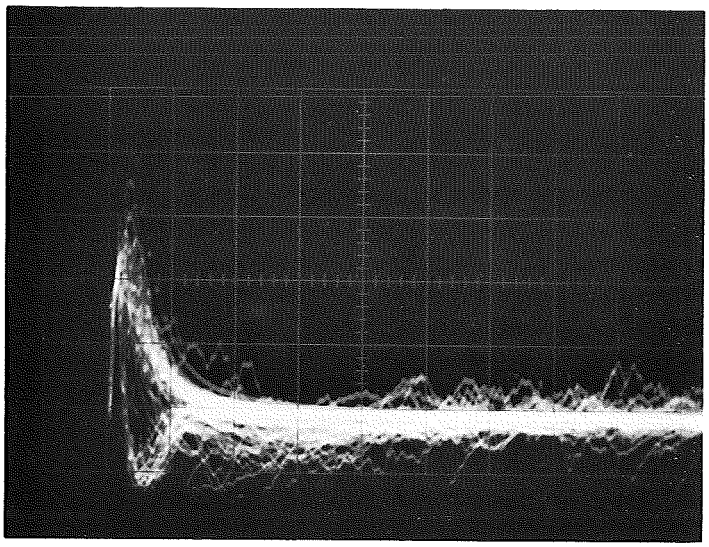

$\frac{dB_\theta}{dt}$ versus t

I_D - 1.0 Ma

P - 20 μ

r - 1 cm

Figure 2.8 Superpositioning of Signals from Two Different Type Arcs

3. Experimental Results

Figure 3.1 shows two examples of the photographic data obtained by the methods described in Chapter 2. As these photographs indicate, the signal obtained is only fairly reproducible even though the pressure, discharge current, coil position, and coil orientation are all held constant during the exposure time of each photograph. The maximum value of $\frac{dB_i}{dt}$ at a particular coil position and orientation $\frac{dB_i}{dt_{MAX}}$ varies by as much as $\pm$ 15%. The time of the first zero crossing of $\frac{dB_i}{dt}$ varies by about $\pm$ 10%. The time of the first zero crossing is significant since it is the time of the occurrence of the maximum value of B_i , $B_{i_{MAX}}$, for a given coil location and orientation.

The variation in signal strength can be attributed partly to the fact that arcs occurring within a very small radius of the coil's center will induce a voltage in the coil large enough to be detected on the oscilloscope. The voltage induced by such arcs will vary slightly in strength with the arcs' distances from the coil. For coil positions within 3 centimeters of the sphere, there is also the previously mentioned interference due to signals induced by the spark-like arcs. Once the oscilloscope has been triggered by a sufficiently large signal, then weaker signals due to the spark-like arcs or distant flash-like arcs can add to the signal displayed on the oscilloscope provided these spurious signals occur within the sweep time of the original triggering signal. The signal in Figure 3.1(a) was recorded

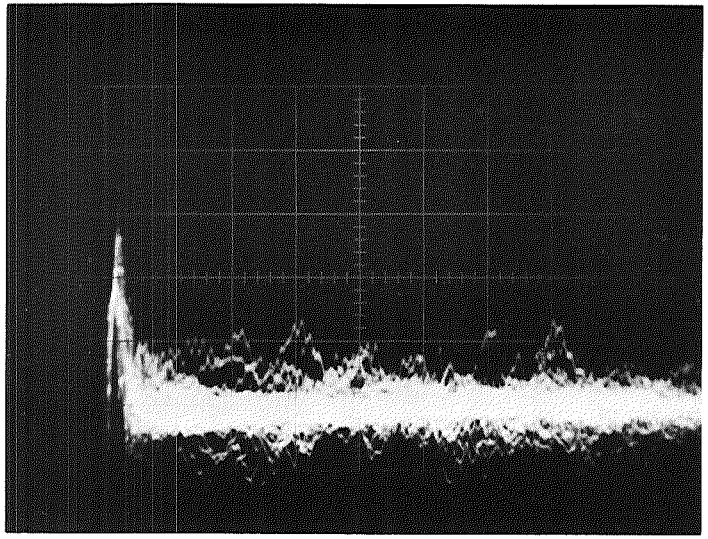

(a)

$\frac{dB_p}{dt}$ versus t

r = 2 cm

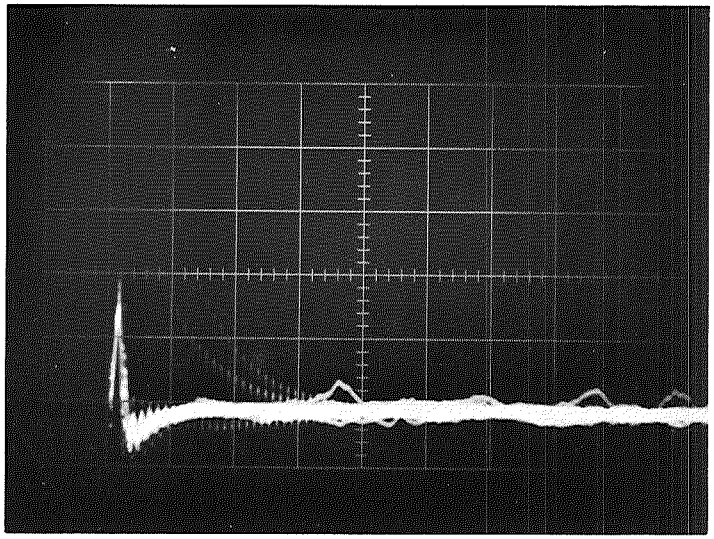

(b)

$\frac{dB_\phi}{dt}$ versus t

r = 6 cm

I_D - 1.0 Ma

P - 10 μ

Figure 3.1 Sample Data

with the coil 2 centimeters from the sphere's surface and, consequently, was much more prone to interference from the spark-like arcs than was the signal shown in Figure 3.1(b) which was recorded with the coil 6 centimeters from the sphere's surface.

In order to label the components of $\frac{d\vec{B}}{dt}$ and $\vec{B}(t)$ that are measured, a reference system is assumed with its center located at the center of the magnetized sphere. Figure 3.2 shows a sketch of this reference system with spherical coordinates being employed. As this figure indicates, the x-y plane of the coordinate system is assumed to lie in the equatorial plane of the sphere. With spherical coordinates, the three components of $\frac{d\vec{B}}{dt}$ that are measured are $\frac{dB_\rho}{dt}$, $\frac{dB_\theta}{dt}$, and $\frac{dB_\phi}{dt}$. The subscript ρ refers to the radial variable, θ refers to the colatitudinal angle, and ϕ refers to the azimuthal angle in the equatorial plane. The mutually orthogonal $\hat{\rho}$, $\hat{\theta}$, and $\hat{\phi}$ directions are indicated in the figure for an arbitrary position P in the equatorial plane. In that plane, $\hat{\theta}$ is always perpendicular to the equatorial plane. Since the arcs originate in the equatorial plane and follow the magnetic field lines of the sphere, the direction of the arcs in the equatorial plane is always the $\hat{\theta}$ direction.

3.1 $\frac{dB_i}{dt}$ and B_i Versus t

Figure 3.3(a) is a sketch of a typical $\frac{dB_i}{dt}$ versus t signal. All the photographs of $\frac{dB_i}{dt}$ versus t contain plots with the same basic shape as that in the figure. The signal always starts at zero

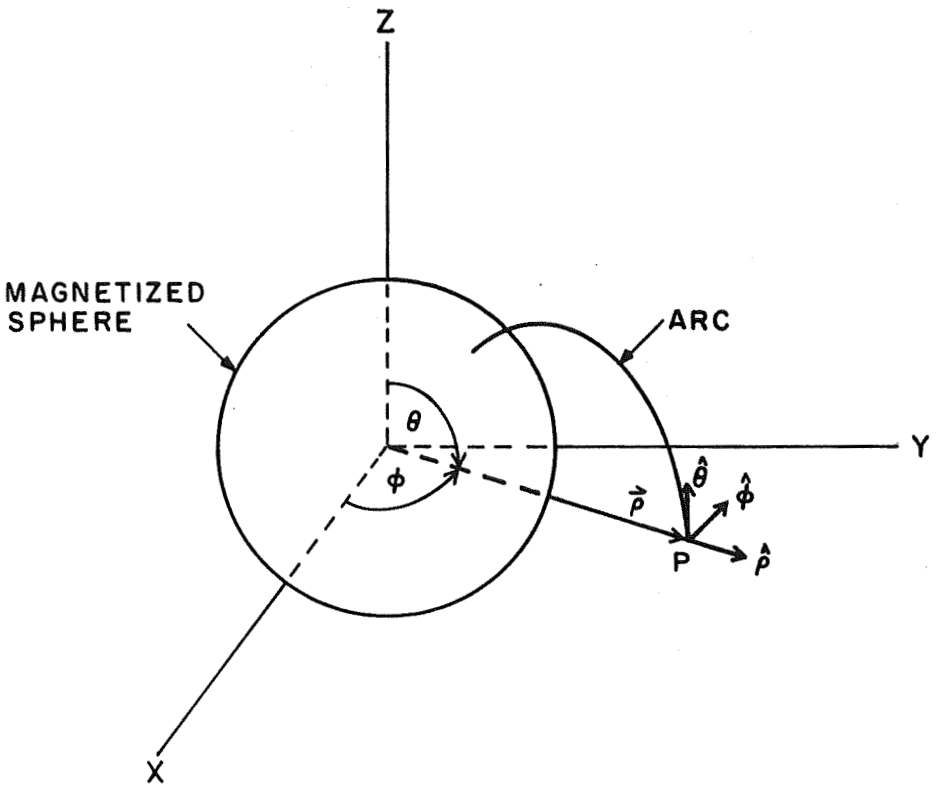

Figure 3.2 Reference System with the Sphere and an Arc Included

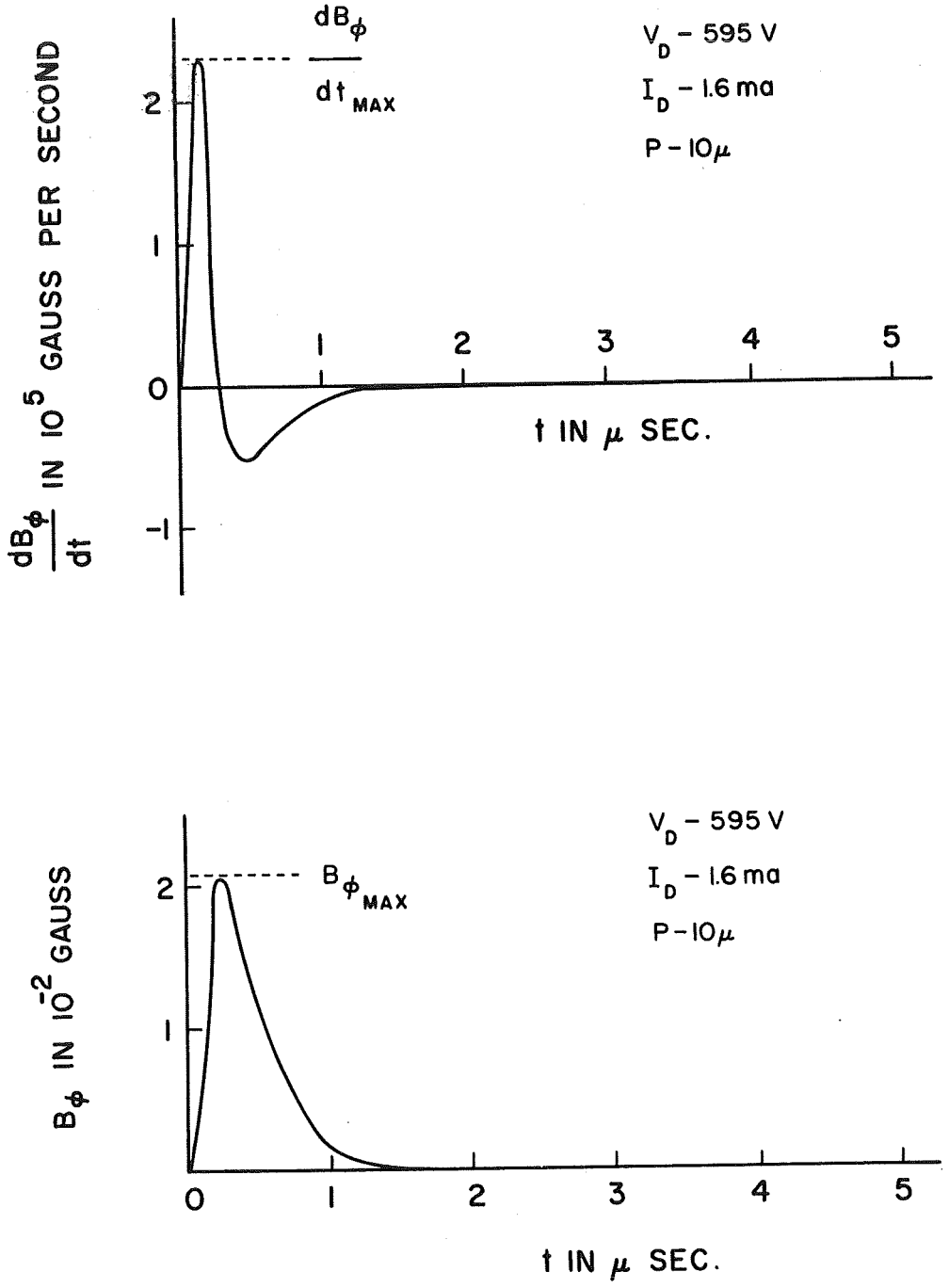

Figure 3.3 Typical Plots of $\frac{dB_i}{dt}$ and B_i Versus t

and initially rises sharply to its maximum value $\frac{dB_i}{dt_{MAX}}$. This maximum always occurs between 0.20 and 0.25 microseconds after the signal begins. Upon reaching $\frac{dB_i}{dt_{MAX}}$, the signal falls almost vertically through zero to a negative value. The zero crossing occurs between 0.22 and 0.28 microseconds after the start of the signal. The minimum value of $\frac{dB_i}{dt}$ always occurs between 0.30 and 0.55 microseconds after the start of the signal. After going through this negative minimum, the signal gradually returns to zero, usually about 2 to 5 microseconds after the start of the signal.

Since all the $\frac{dB_i}{dt}$ signals have similar shapes, all the $B_i(t)$ versus t plots have essentially similar shapes. Figure 3.3(b) shows a typical $B_i(t)$ versus t curve. This figure is obtained by graphically integrating the curve in Figure 3.3(a). $B_{i_{MAX}}$ occurs at the time of the first zero crossing of $\frac{dB_i}{dt}$. $B_i(t)$ does not change sign throughout the duration of the signal and it goes to zero finally as $\frac{dB_i}{dt}$ goes to zero.

3.2 $\frac{dB_i}{dt_{MAX}}$ Versus r

Figures 3.4 to 3.6 show plots of $\frac{dB_i}{dt_{MAX}}$ versus r, the radial distance of the coil from the sphere's surface. These plots are obtained by choosing the largest value of $\frac{dB_i}{dt}$ that occurs in each photograph. All of the plots shown are for $\frac{dB_i}{dt_{MAX}}$ in the equatorial plane. The discharge conditions appropriate to each plot are presented in the figures. The values of $\frac{dB_i}{dt_{MAX}}$ presented have an uncertainty of about $\pm$ 10%.

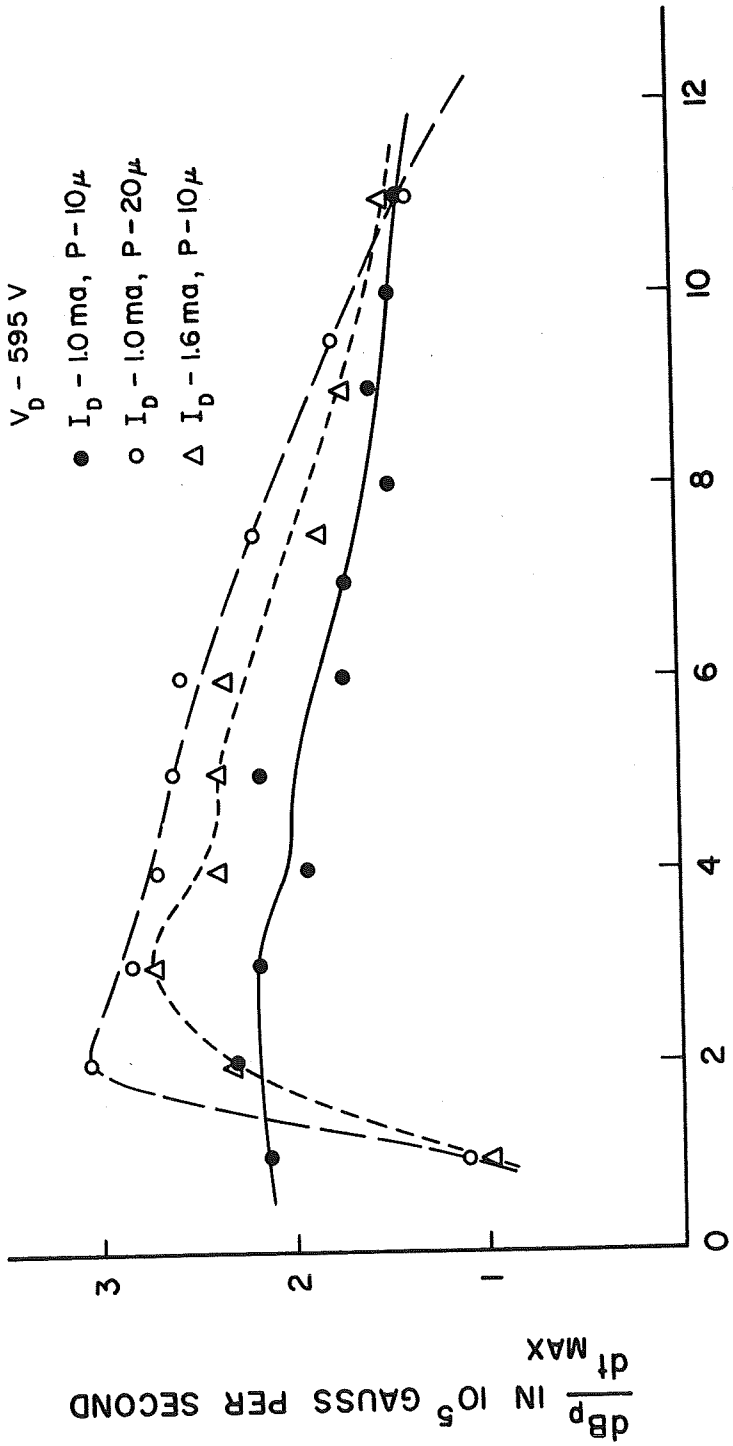

Figure 3.4 $\frac{dB_\rho}{dt_{MAX}}$ Versus r

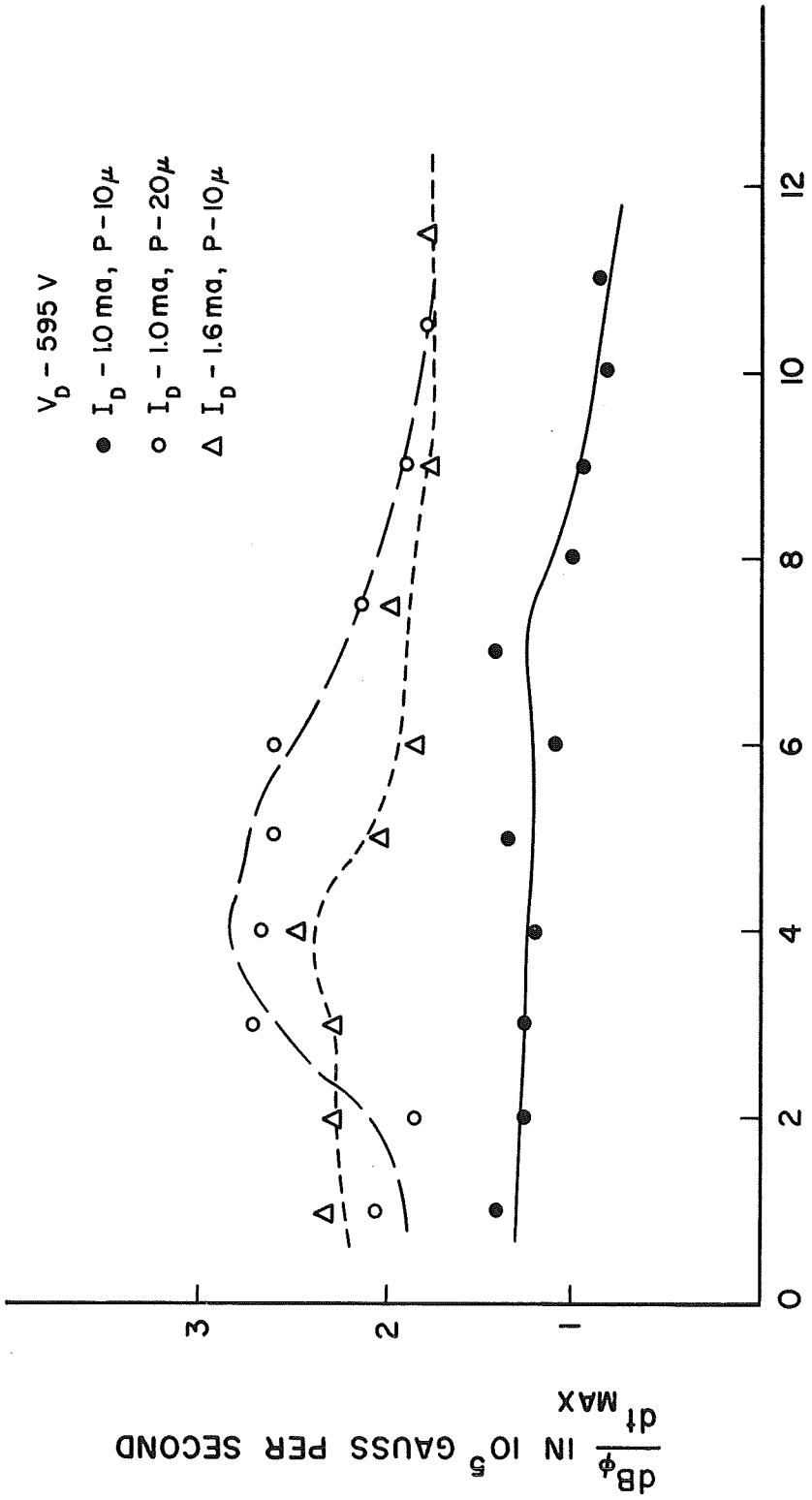

Figure 3.5 $\frac{dB_\phi}{dt}_{MAX}$ Versus r

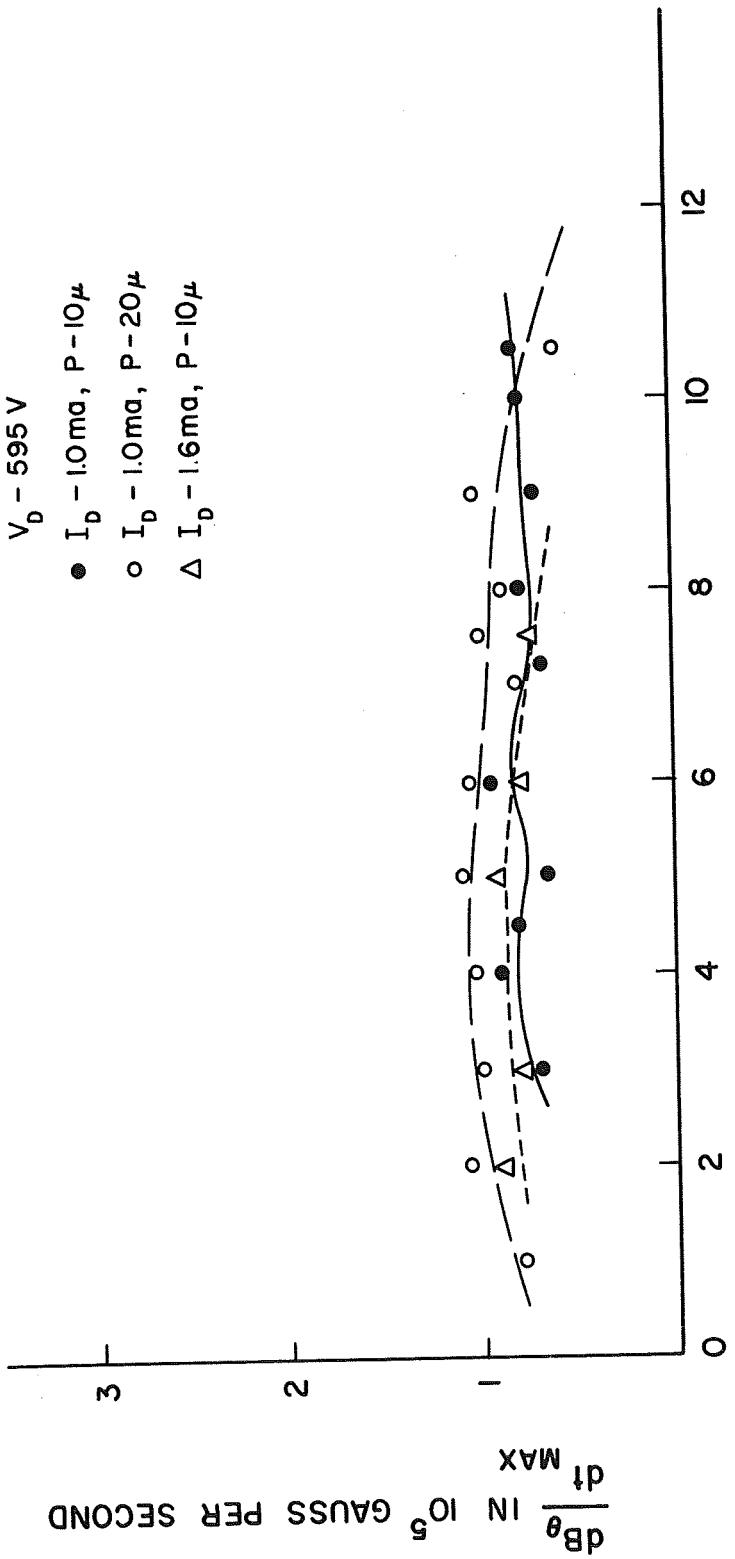

Figure 3.6 $\frac{dB_\theta}{dt_{MAX}}$ Versus r

3.3 $B_{i_{MAX}}$ Versus r

The fact that all the $\frac{dB_i}{dt}$ versus t curves have the same basic shape as the plot in Figure 3.3(a) is used to facilitate the graphical integration of $\frac{dB_i}{dt}$. The positive portion of the signal, with its sharp rise to a maximum and then its almost vertical drop through zero, has a markedly triangular shape. The integration of the positive part of the $\frac{dB_i}{dt}$ signal is performed by approximating that portion of the $\frac{dB_i}{dt}$ curve by a triangle and then computing the area of the triangle from its altitude, $\frac{dB_i}{dt_{MAX}}$, and the width of its base. Since $B_{i_{MAX}}$ is equal to the area under the $\frac{dB_i}{dt}$ versus t curve from $t = 0$ to the time of the first zero crossing of $\frac{dB_i}{dt}$, the area of the triangle is equal to $B_{i_{MAX}}$ for the particular coil location and orientation being considered. The values obtained by this method have an uncertainty of about $\pm$ 15% due principally to undertainty in the exact time of the first zero crossing of $\frac{dB_i}{dt}$ and in the exact value of $\frac{dB_i}{dt_{MAX}}$. Figure 3.7 shows a sample plot of $B_{\rho_{MAX}}$ versus r with this uncertainty represented by error flags. In the plots that follow, these error flags are omitted for the sake of clarity. Figures 3.8 to 3.10 are plots of $B_{i_{MAX}}$ versus r. The discharge conditions and component of $B_{i_{MAX}}$ appropriate to each plot are given in the figure. The characteristics of the plots of both $B_{i_{MAX}}$ and $\frac{dB_i}{dt_{MAX}}$ versus r are discussed in Chapter 4.

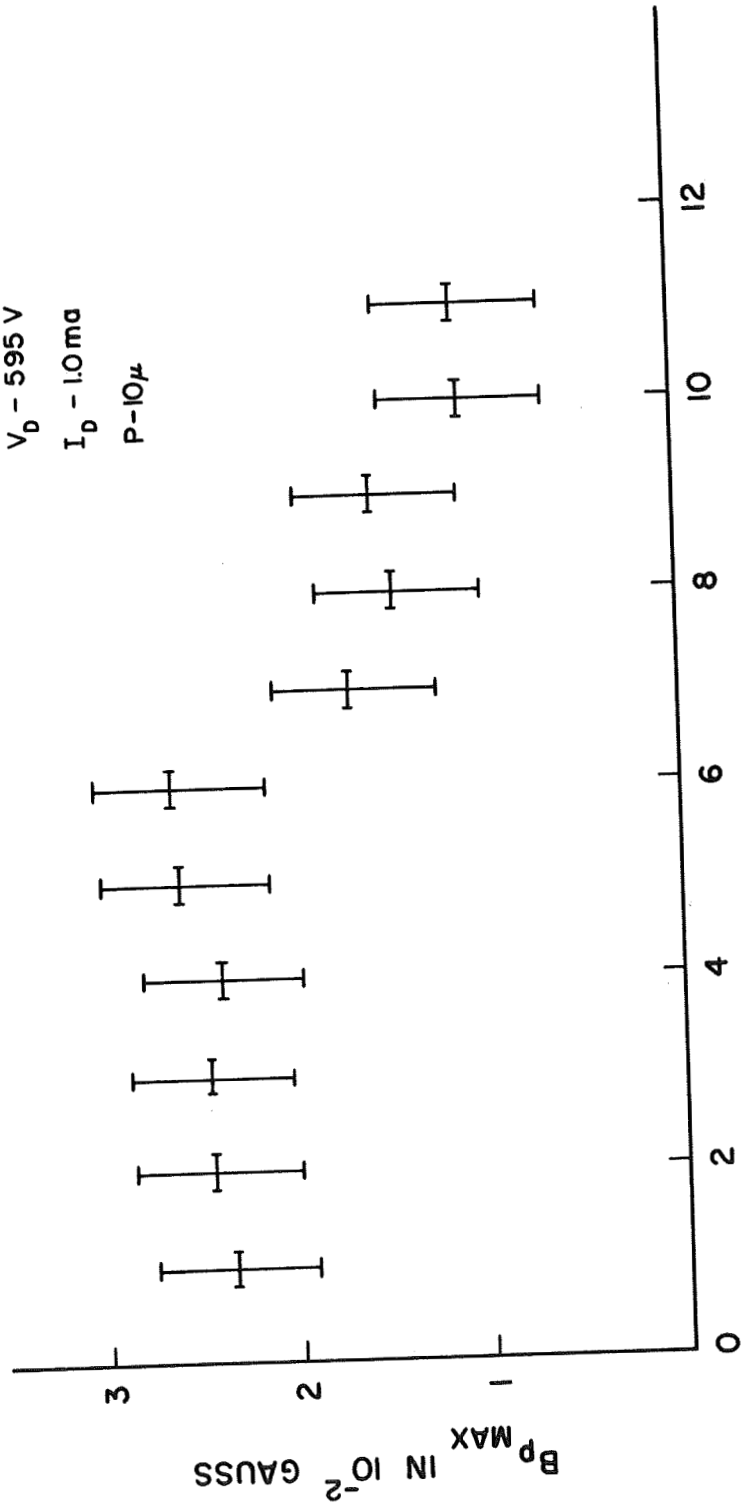

Figure 3.7 $B_{\rho_{MAX}}$ Versus r with Error Flags

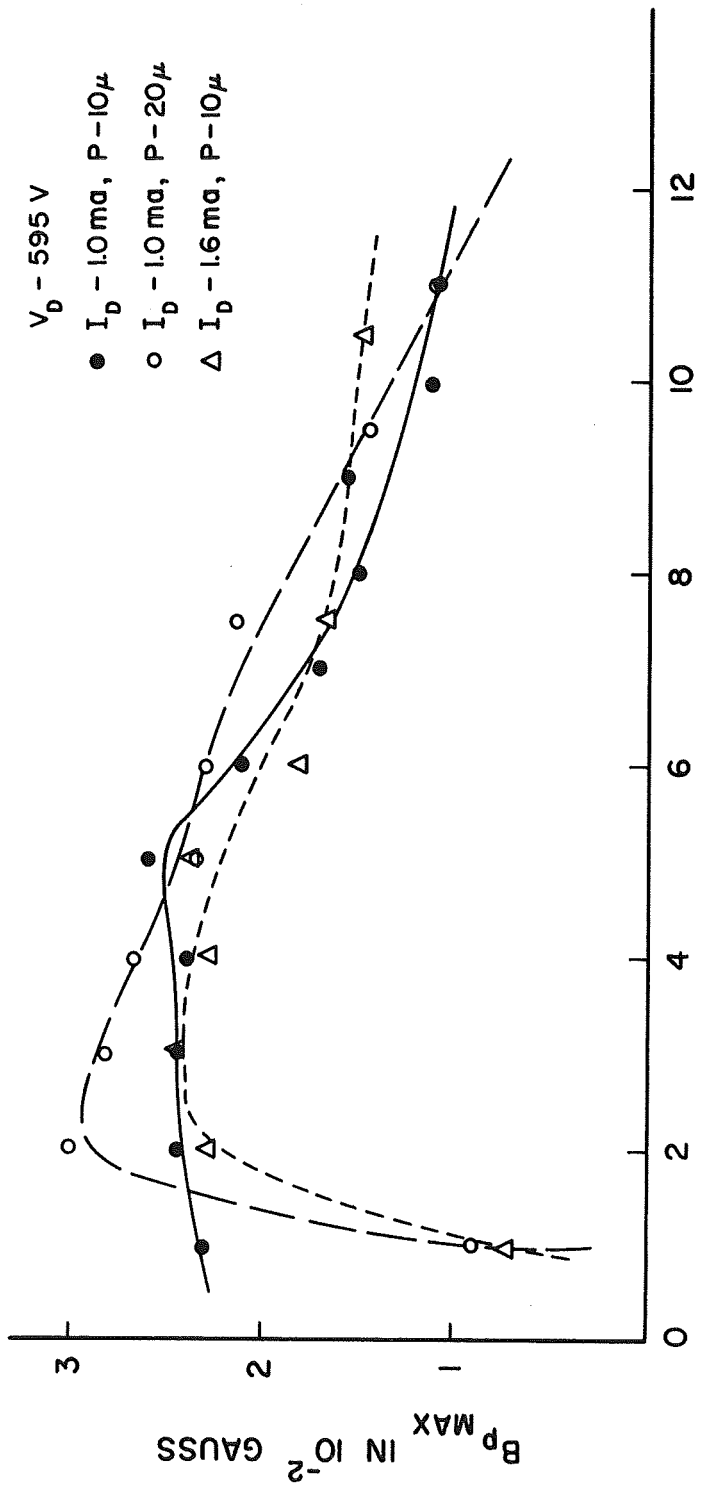

Figure 3.8 $B_{\rho_{MAX}}$ Versus r

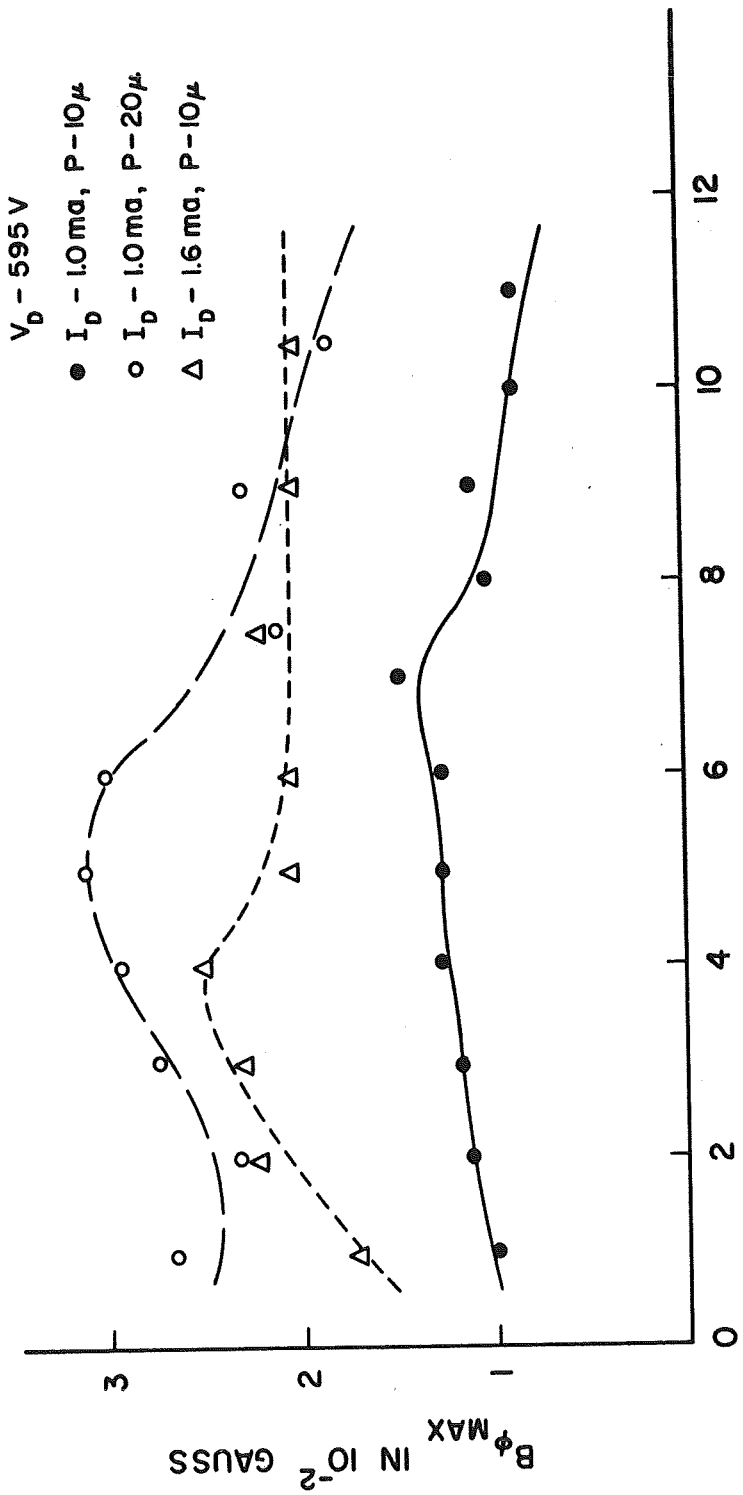

Figure 3.9 $B_{\phi_{MAX}}$ Versus r

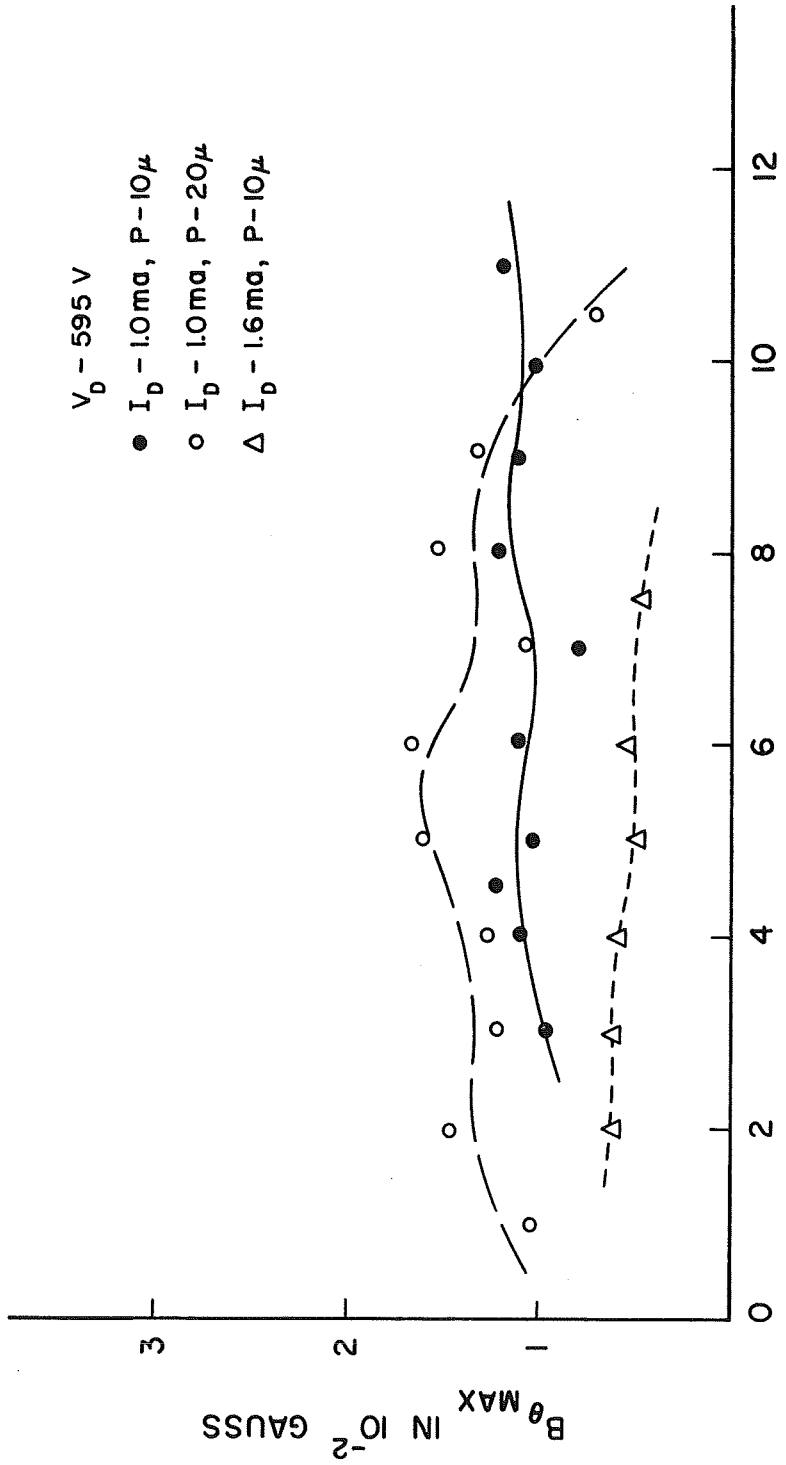

Figure 3.10 $B_{\theta_{MAX}}$ Versus r

4. Summary and Discussion

From the data presented in Chapter 3, several characteristics of the behavior of the arcs' transient magnetic fields are observed. The values of $\frac{dB_\phi}{dt}_{MAX}$ and $\frac{dB_\rho}{dt}_{MAX}$ are usually about two to three times as large as $\frac{dB_\theta}{dt}_{MAX}$ for corresponding coil positions and discharge conditions. Similarly, the magnitudes of $B_{\phi_{MAX}}$ and $B_{\rho_{MAX}}$ are about twice as great as $B_{\theta_{MAX}}$. None of the plots of $\frac{dB_\theta}{dt}_{MAX}$ or $B_{\theta_{MAX}}$ versus r contains a well-defined maximum, which indicates that both $\frac{dB_\theta}{dt}_{MAX}$ and $B_{\theta_{MAX}}$ are fairly constant with respect to variation in r.

The magnitudes of $\frac{dB_\rho}{dt}_{MAX}$ and $\frac{dB_\phi}{dt}_{MAX}$ increase when either the discharge current or the pressure is increased. The plots of $B_{\phi_{MAX}}$ versus r show this same increase in magnitude with increasing pressure or discharge current. The plots of $B_{\rho_{MAX}}$ versus r show that, while $B_{\rho_{MAX}}$ increases when the pressure is increased, its magnitude appears to be unaffected by an increase in the discharge current.

The temporal variations of the magnetic field last for about 4 to 5 microseconds. Furthermore, $B_i(t)$ never changes sign. The discussion which follows presents some possible explanations of these spatial and temporal characteristics.

The fact that the ϕ and θ components of $\frac{d\vec{B}}{dt_{MAX}}$ and $\vec{B}_{MAX}$ are usually two or three times as large as the θ component can be explained on the basis that all the magnetic field measurements were made in the equatorial plane. In this plane, the direction of propagation of the arcs is perpendicular to the equatorial plane and parallel to the $\hat{\theta}$ direction. One expects that $\frac{dB_\theta}{dt_{MAX}}$, being the component of $\frac{d\hat{B}}{dt_{MAX}}$ in the direction of the arcs, will be less than either $\frac{dB_\phi}{dt_{MAX}}$ or $\frac{dB_\rho}{dt_{MAX}}$, which are components of $\frac{d\vec{B}}{dt_{MAX}}$ perpendicular to the arcs. The same reasoning applies to the magnitude of $B_{\theta_{MAX}}$ compared to that of $B_{\phi_{MAX}}$ or $B_{\rho_{MAX}}$ and to the fact that $\frac{dB_\theta}{dt_{MAX}}$ and $B_{\theta_{MAX}}$ are relatively constant with respect to r.

The increase in $\frac{dB_\rho}{dt_{MAX}}$ and $\frac{dB_\phi}{dt_{MAX}}$ with increasing discharge current or pressure and the existence of a maximum in their spatial variations can be explained by considering what mechanisms can cause changes in the current densities of the arcs. The arcs appear to originate in the plasma belt and are apparently caused by some sort of instability in the equatorial current. It is not clear at this time exactly what the instability is; however, the present experimental results are found to be consistent with preliminary explanations offered by Quinn and Fiorito based on either of two separate theories of Alfven and of Swift. Swift's theory first considers a longitudinal ring current in a dipolar magnetic field, subjected to an electric

field which may be fluctuating or steady-state and is transverse to the magnetic field. It can be shown that, under the proper conditions, the longitudinal current may become unstable, causing growing ion-acoustic waves. By inhibiting current flow, these waves cause turbulent heating and an acceleration of charged particles along the magnetic field lines. The amount of energy available for an arc, according to Swift's theory, increases with plasma density and electric field. This is an agreement with the data in this work indicating that the maximum in the transient magnetic fields occurs near the region of maximum plasma density and radial electric field.

Alfven's theory is based on the assumption that a neutral gas moving in a plasma will become ionized when its velocity with respect to the plasma is such that its kinetic energy is equal to its ionization energy. It can be shown that the amount of energy produced by this ionization mechanism increases with the amount of energy transferred to electrons in the plasma via electron-ion Coulomb collisions. The amount of energy transferred by collisions increases with the charged-particle density and the mean velocities of the charged particles with respect to each other. Since an increase in the discharge current can be interpreted as either an increase in the density or mean velocities of the charged particles and an increase in pressure can be interpreted as an increase in charged-particle density for low pressures, the increases in $\frac{dB_\rho}{dt_{MAX}}$ and $\frac{dB_\phi}{dt_{MAX}}$ with increasing discharge current and pressure seem consistent with the basic aspects of Alfven's theory.

The fact that the transient fields of the arcs last for only 4 or 5 microseconds while the potential fluctuations measured by Quinn and Fiorito last the order of tens of milliseconds needs further examination. Using essentially the same type of discharge configuration as that described herein, Quinn and Fiorito measured the time variation of the floating potential in the equatorial plasma belt during arc instabilities. All their potential measurements in the equatorial plane have the same basic shape that is shown in Figure 4.1. The starting point and minimum potential to which the curve returns after the arc occurrence is the steady-state potential. The maximum value of the curve is zero volts, the same potential as the grounded anode.

This data indicates the effect of an arc which lasts for tens of milliseconds, while the data presented herein indicates that an arc lasts for only 4 or 5 microseconds. Thus, the potential fluctuations indicate the changes in the plasma belt during the production and occurrence of an arc rather than the time properties of the arc itself. The magnetic field measurements, on the other hand, indicate the transient behavior of the field associated with the current density of the arc. The lifetime of this magnetic field is the lifetime of the current comprising the arc.

One further piece of experimental information, the observation of steady-state plasma oscillations in the kilohertz range by Schmidt, allows one to develop the following description of the instability.

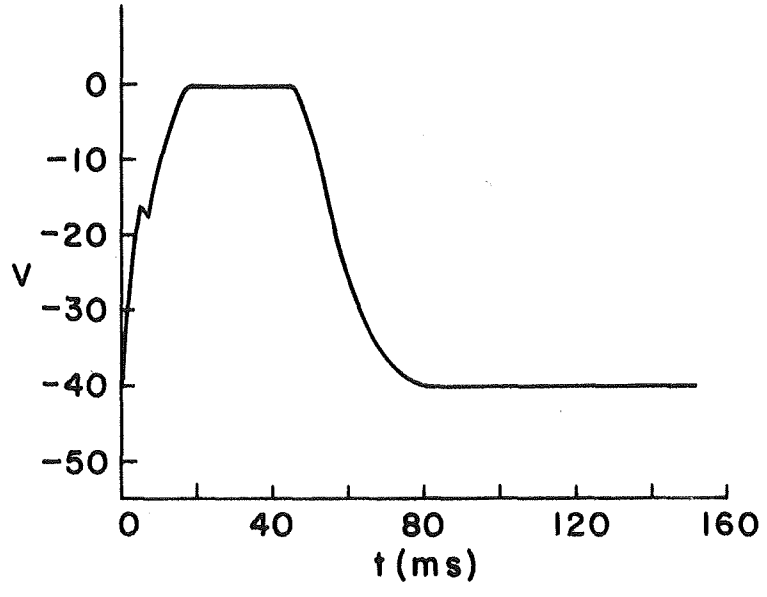

Figure 4.1 Typical Time Variation of the Potential at an Arbitrary Point in the Plasma

The potential of a point in the equatorial plasma belt increases to the anode potential in a time characteristic of many oscillation periods. Under the appropriate conditions, this potential is sufficient to ignite an arc which is quenched in a few microseconds. The potential then relaxes to its initial equilibrium value in a time characteristic of several oscillation periods.

While this prior description of the instability phenomena is qualitatively consistent with the three separate experimental investigations, namely, the electric probe, the magnetic probe, and the noise measurements, there is no definitive or quantitative evidence available at this time to characterize the exact nature of the instability or its possible geophysical relevance. Such evidence will be obtained only in experiments where one has more adequate control of such important parameters as plasma density, temperature, neutral pressure, and electric field.

BIBLIOGRAPHY

Alfven, H., On the Origin of the Solar System, Oxford University Press, Oxford, 1954.

Clauser, F., ed., Symposium on Plasma Dynamics, Addison-Wesley Publishing Company, Inc., Reading, Massachusetts, 1960.

Colgate, S., J. Ferguson, and H. Furth, 2nd U. N. Conference on the Peaceful Uses of Atomic Energy, 32, 129, 140, 1958.

Del Torro, V., Principles of Electric Engineering, Prentice-Hall, Inc., Englewood Cliffs, New Jersey, 1965.

Glasstone, S., and R. Lovberg, Controlled Thermonuclear Reactions, D. Van Nostrand Company, Inc., Princeton, New Jersey, 1960.

Guthrie, A., and R. Wakerling, ed., The Characteristics of Electric Discharges in Magnetic Fields, McGraw-Hill, New York, 1949.

Heald, M. and C. Wharton, Plasma Diagnostics with Microwaves, John Wiley and Sons, Inc., New York, 1965.

Huddlestone, R., and S. Leonard, ed., Plasma Diagnostic Techniques, Academic Press, New York, 1965.

Landshoff, R., ed., The Plasma in a Magnetic Field, Stanford University Press, Stanford, California, 1958.

Longmire, C., Elementary Plasma Physics, Interscience Publishers, New York, 1963.

Lovberg, R., The Proceedings of the 6th International Conference on Ionization Phenomena in Gases, Paris, 1963, North-Holland, Amsterdam, 1964.

Quinn, R., Laboratory Observations of Plasma Instabilities in a Dipole Magnetic Field, Nature, 208, 376, 1965.

Quinn, R. and C. Chang, Laboratory Observations of a Stable Plasma Trapped in a Permanent Dipolar Magnetic Field, J. Geophys. Res., 72, 253, 1966.

Quinn, R. and R. Fiorito, Investigation of Laboratory Plasma Instabilities in a Dipole Magnetic Field, J. Geophys. Res., 72, 1611, 1967.

Roshon, D., Microprobe for Measuring Magnetic Fields, Rev. Sci. Instr., 33, 2, 201, 1962.

Schmidt, P., proposed Sci. Rep., Ionosphere Research Laboratory, The Pennsylvania State University, to be published in 1969.

Swift, D., A Mechanism for Energizing Electrons in the Magnetosphere, J. Geophys. Res., 70, 3061, 1965.

Tuck, J., The Proceedings of the 2nd International Conference on the Peaceful Uses of Atomic Energy, Geneva, 1958, Vol. 32, I. D. S. Columbia University Press, New York, 1959.

Twardeck, T., An Investigation of Microwave Interaction with a Plasma Confined in a Dipolar Magnetic Field, Sci. Rep. 320, Ionosphere Research Laboratory, The Pennsylvania State University, 1968.

von Engel, A., Ionized Gases, Clarendon Press, Oxford, England, 1955.